

# A fully sampled $\lambda 21$ cm linear polarization survey of the southern sky

J. C. Testori<sup>1,2</sup>, P. Reich<sup>1</sup>, and W. Reich<sup>1</sup>

<sup>1</sup> Max-Planck-Institut für Radioastronomie, Auf dem Hügel 69, 53121 Bonn, Germany  
e-mail: [wreich@mpi-fr-bonn.mpg.de](mailto:wreich@mpi-fr-bonn.mpg.de)

<sup>2</sup> Instituto Argentino de Radioastronomía, C.C.5 (1894) Villa Elisa, Argentina

Received 12 October 2007 / Accepted 25 February 2008

## ABSTRACT

**Context.** Linear polarization of Galactic synchrotron emission provides valuable information on the Galactic magnetic field and on the properties of the Galactic magneto-ionic medium. Polarized high-latitude Galactic emission is the major foreground for polarization studies of the cosmic microwave background.

**Aims.** We present a new southern-sky  $\lambda 21$  cm linear polarization survey, which complements the recent  $\lambda 21$  cm DRAO northern sky polarization data.

**Methods.** We used a 30-m telescope located at Villa Elisa/Argentina to map the southern sky simultaneously in continuum and linear polarization.

**Results.** We present a fully sampled map of linearly polarized emission at  $\lambda 21$  cm of the southern sky for declinations between  $-10^\circ$  and  $-90^\circ$ . The angular resolution of the survey is  $36'$  and its sensitivity is 15 mK (rms-noise) in Stokes  $U$  and  $Q$ . The survey's zero-level has been adjusted to that of the recent DRAO 1.4 GHz linear polarization survey by comparing data in the region of overlap between  $-10^\circ$  and  $-27^\circ$ .

**Conclusions.** The polarized southern sky at 1.4 GHz shows large areas with smooth low-level emission almost uncorrelated to total intensities indicating that Faraday rotation originating in the Galactic interstellar medium along the line of sight is significant at 1.4 GHz. The southern sky is much less contaminated by local foreground features than is the northern sky. Thus high-frequency observations of polarized cosmic microwave emission are expected to be less affected. The percentage polarization of the high-latitude emission is low, which seems to be an intrinsic property of Galactic emission.

**Key words.** polarization – radiation mechanisms: non-thermal – ISM: magnetic fields

## 1. Introduction

Linear polarization surveys for large sections of the northern sky and the southern sky were carried out in the years following the first detection of linear polarization in the early sixties by [Westerhout et al. \(1962\)](#) and [Wielebinski et al. \(1962\)](#). Most observations were made at 408 MHz. 1.4 GHz was the highest frequency used (see [Reich 2006](#), for a recent review). All these early surveys were incompletely sampled and limited in sensitivity. However, time consuming but essential absolute zero-level determination was provided ([Brouw & Spoelstra 1976](#)). Although observed in the sixties, these data are still helpful for present experiments suffering from limited telescope time or instrumental limitations. The recent DRAO survey at 1.42 GHz ([Wolleben et al. 2006](#)) marks a revival of large-scale polarization sky surveys, because it provides a much denser sampling and higher sensitivity than the early Dwingeloo surveys by [Brouw & Spoelstra \(1976\)](#), although it adopts their absolute zero-level. Traditionally, the southern sky, where nearly all observations come from the Parkes 64-m telescope, is less intensely studied than the northern sky. For the southern sky, polarization data were collected at 408 MHz in the early sixties ([Mathewson et al. 1966a](#)). Also, observations at 620 MHz and a few measurements at 1.41 GHz were made by [Mathewson et al. \(1966b\)](#). From their 1.41 GHz observations, 37 selected measurements of the diffuse Galactic emission were published, where polarized intensities exceed 200 mK  $T_B$ .

During the past decade, the interest in Galactic polarization surveys increased as they show features with no correspondence in the total intensity data. The observed polarization structures result from Faraday rotation effects along the line of sight, thereby revealing insights into the properties of the Galactic magneto-ionic medium. It was also realized that sensitive cosmic microwave background studies aiming to detect polarization signals from the early universe might suffer from polarized Galactic synchrotron radiation as the dominant foreground.

[Reich \(2006, and references therein\)](#) has reviewed the present status of Galactic polarization surveys. Most recent projects are limited to observations of the Galactic plane either using large single-dish telescopes like the Effelsberg 100-m or the Parkes 64-m telescopes, where arcmin angular resolutions are obtained at  $\lambda 21$  cm or  $\lambda 11$  cm, or very recently with the Urumqi 25-m telescope at  $\lambda 6$  cm ([Sun et al. 2007a,b](#)). In addition, considerable efforts have been made for 1.4 GHz polarization surveys with an angular resolution of about  $1'$  using synthesis telescopes e.g. the Canadian Galactic plane survey, CGPS ([Taylor et al. 2003](#)) and the Southern Galactic plane survey, SGPS ([Gaensler et al. 2001](#)). Small-scale polarization structures with no total intensity counterpart result from Faraday rotation and depolarization effects in the interstellar medium. Their interpretation is not possible without adding the missing large-scale components and adjusting the maps to the correct absolute zero-level (see e.g. [Reich 2006](#)). The 1.4 GHz DRAO northern

sky survey carried out with a 26-m telescope (Wolleben et al. 2006) adopted the absolute zero-level from the Dwingeloo polarization survey by Brouw & Spoelstra (1976). Its inclusion is necessary for the *Effelsberg Medium Latitude Survey* (EMLS) (W. Reich et al. 2004), which covers the Galactic plane out to  $\pm 20^\circ$  at an angular resolution of  $9.4'$ . The combined result from the single-dish surveys is used to adjust the CGPS interferometric data. Only a combination of all three surveys gives the complete polarization information on all spatial scales down to one arcminute for the area covered by the CGPS (Landecker et al., in prep.).

We carried out a fully sampled southern sky survey in total intensity at  $\lambda 21$  cm using a Villa Elisa 30-m telescope (Testori et al. 2001; Reich et al. 2001). Linear polarization data were collected simultaneously during these observations. We describe the reduction of these data, which differs from the reduction of the total intensity measurements, and present the resulting maps. The Villa Elisa polarization survey is the southern complement to the northern DRAO survey. Both surveys match in angular resolution and sensitivity. A combination of both surveys to an all-sky map is described in a companion paper by Reich et al. (in prep.).

## 2. Observations and data reduction

The southern sky was simultaneously mapped in total intensity and linear polarization using one of the two 30-m telescopes of the Instituto Argentino de Radioastronomía located at Villa Elisa (Argentina) at  $\lambda 21$  cm. The receiving system has already been described in some detail by Testori et al. (2001), so we only give a brief summary of its main features.

The receiver box is located in the prime focus of the 30-m telescope and consists of a corrugated conical horn followed by a turnstile providing the left-hand and right-hand circularly polarized components of the received signal. The polarization isolation of this device should be better than 30 dB. The circularly polarized components are connected to two uncooled low-noise amplifiers with a noise temperature of 60 K at room temperature. The system noise towards the coldest regions of the sky was measured to be about 90 K. An internal noise tube provided gain calibration of the receiving system and was injected for half of the observing time. At the IF-stage (123.5 MHz), the two signals were filtered with a phase-matched pair of filters and fed into an IF-polarimeter. To minimize the phase drift in the polarimeter that is caused by differential changes in electrical length of both receiver channels, low attenuation cables were used for the IF and LO between the front-end and the control room. This polarimeter is a copy of the standard narrow-band IF-polarimeter used at the MPIfR Effelsberg 100-m telescope. Another copy of this polarimeter was used for the DRAO 1.4 GHz polarization survey by Wolleben et al. (2006). The polarimeter provides output proportional to all Stokes parameters. Both  $U$  and  $Q$  are obtained from analogue correlation of the left-hand and right-hand circular antenna signals.

Testori et al. (2001) already described the observational procedure of the  $\lambda 21$  cm southern sky survey and also its calibration and reduction for the total intensity channels. The results of the total intensity survey were published by Reich et al. (2001). In brief, the southern sky was mapped by applying the “*Nodding Scan Technique*” (Haslam et al. 1974), where the telescope continuously moves up and down in elevation along the local meridian. Up and down scans were individually recorded, and the earth’s rotation provides a full coverage in right ascension. Each day the observations were started about 1 minute later in sidereal

time to provide a full sampling after 16 nights. The telescope moved with  $10^\circ/\text{min}$  in elevation corresponding to a declination range between  $-90^\circ$  and  $-10^\circ$ . Each up or down scan was observed at least twice. A four-phase switching scheme of  $4 \times 60$  ms was used, where the calibration signal was added to the antenna signal for two phases. During two phases (one of them includes the calibration signal), a  $180^\circ$  phaseshift was added to remove second-order terms in the correlated polarization signals. This front-end switching scheme provides a receiver gain control on short time scales.

The polarization data used here were exclusively observed between 1987 and 1989 at 1435 MHz, while observations made between 1993 and 1994 were also used for the total intensity survey. The latter has a centre frequency of 1420 MHz and used a bandstop filter to reject the Galactic HI-line, but the filter affects the polarization data so that they are not included here.

A number of strong calibration sources were observed every day. The main calibration sources for the survey were PKS 0518-45 (Pictor A) and PKS 0915-11 (Hydra A). For the list of secondary calibration sources see Table 3 of Testori et al. (2001). The phase setting of the polarimeter was controlled over a highly stable calibration signal, which was injected for 50% of the observing time into the RHC and the LHC channel before amplification (see Testori et al. 2001, Fig. 1). The calibration signal was then extracted from the two linear polarization channels of the polarimeter. Its ratio was used to calculate the appropriate time-dependent polarization angle variations caused by the receiving system, which is measured relative to the polarization angle as defined by the calibration signal injection. The data of two polarization channels were corrected accordingly, and the polarization angle reference frame was kept constant over the observing period to high precision. The polarization angle transformation into astronomical coordinates was provided by a comparison with polarized calibration sources (Sect. 2.4).

Testori et al. (2004) have already described the principal steps of data reduction and calibration applied to the polarization data. The two polarization channels from about 6500 declination scans were edited for all kind of interference or distortions following the methods applied for the total intensity data after having sorted out about 300 scans that are too strongly distorted. The mean intensity for each scan was set to zero. Raw maps were calculated from the edited scans, where the coordinates are starting time and elevation. “Scanning effects”, e.g. baseline distortions of individual scans caused by receiver drifts or weather effects, were suppressed by using the method of “unsharp masking” described by Sofue & Reich (1979). This iterative destriping technique removes individual distortions in a map relative to its surroundings by fitting first and second order polynomials to them. This is not always sufficient in case that “scanning effects” vary on timescales shorter than the 8-min duration of one meridian scan. In that case distortions might not be well-fitted by polynomials of second order and residuals are left, which imply that for the  $80^\circ$  long scans local distortions extending up to several degrees are not fully corrected. These remaining “scanning effects” can be clearly identified in low-emission regions in the final maps. We avoid any further processing to suppress these features, as it cannot be ruled out that sky emission is affected by these procedures. The amplitude differences between neighbour scans may reach  $50 \text{ mK } T_B$ . Because striping effects distribute randomly, they almost disappear after smoothing the maps to angular resolutions of  $60'$  to  $90'$ .

## 2.1. Ground radiation profiles

Ground radiation is a major contribution to the polarized signals observed. It is picked up by the telescope’s sidelobes and varies with position of the telescope. The Villa Elisa scans are all observed at the local meridian, so that ground radiation shows up only as a function of elevation. The raw maps constructed from up and down scans of both polarization channels were used to extract a common elevation-dependent scan. The problem is the separation of polarized sky emission, whose sky distribution is largely unknown, from the radiation picked up from the ground. We assumed that the Stokes parameter  $U$  and  $Q$  average to zero over 24 h in right ascension, which we think is a reasonable assumption to start with. In addition we assumed that the ground radiation is constant in time. Ground radiation is picked up by weak far-sidelobes and is thus expected to vary smoothly with elevation. In a first step we separated large-scale from small-scale structures by applying the “*BackGround Filtering (BGF)*” method as described by Sofue & Reich (1979). We tested various filters and finally used a  $10^\circ \times 6^\circ$  wide filter in right ascension and declination, which seems appropriate to extract the ground radiation emission component. From the map of the large-scale components, we averaged all data for each elevation by excluding excessive values believed to be attributed to sky emission and obtained ground radiation profiles separately for the up and down scans for the two polarization channels as shown in Fig. 1. The profiles shown have arbitrary temperature offsets. We obtained very similar profiles for up and down scans for both channels, which deviate by just a few mK. This difference indicates the level of uncertainty introduced by this correction step, which is less than the noise level in the  $U$  and  $Q$  maps and thus not a limiting factor for the results obtained.

The total intensity ground radiation curves (Fig. 3 in Testori et al. 2001) show a rapid increase in the ground radiation picked up towards  $-90^\circ$ . This ground radiation behaviour is reflected in the increase in the ground radiation polarization profile as well, although on a much lower level. The shape and the amplitudes of the polarized ground radiation profiles were constant during the period of observations.

## 2.2. Calibration sources and instrumental polarization

Significant instrumental polarization was observed from known unpolarized sources, such as the HII-regions RCW 16, 27, 36, 38, and 42 and the radiogalaxy Hydra A, which has 0.1% polarization (Gardner et al. 1975). We identified cross-talk from the total intensity channels into the two polarization channels as the main reason. The overall instrumental percentage polarization was determined to be 8.8%, which splits into 4.9% for Stokes  $U$  and 7.3% for Stokes  $Q$ . These values were very stable during the entire survey observations as controlled by daily calibration source measurements.

The measured isolation of the turnstile in the lab, which was quoted by Testori et al. (2001) to be better than 30 db, does not seem to be the main source of instrumental polarization. The main additional leakage seems to have happened by a mismatch of the IF-polarimeter. This type of device is the standard narrow-band polarimeter used at the Effelsberg 100-m telescope, where the overall instrumental polarization is quite low. For instance, the instrumental polarization of the  $\lambda 11$  cm polarization survey of the Galactic plane was measured as about 1% (Junkes et al. 1987).

Testori et al. (2004) have shown an example of a large Stokes  $U$ -map both with and without instrumental correction, where a

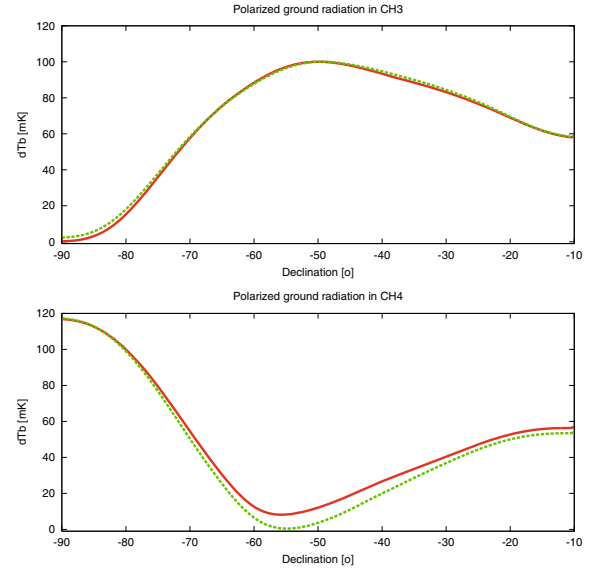


**Fig. 1.** The derived ground radiation profiles from the backend polarization channels “CH3” and “CH4” are shown separately for the up (dashed line) and down (solid line) scans. The zero-level is arbitrary. “CH3” and “CH4” correspond to Stokes  $-U$  and  $Q$  after rotation by the instrumental polarization angle offset, which was determined from Parkes observations of polarized sources as described in Sect. 2.4. The zenith of the telescope is at  $-55^\circ$  declination.

section of the Galactic plane clearly shows up in the original polarization data, but vanishes almost completely after applying the instrumental correction. Very low polarized emission along the Galactic plane is in fact expected at 1.4 GHz, because the recent WMAP polarization maps at 22.8 GHz and at higher frequencies (Page et al. 2007) show a very small amount of polarized emission along the southern Galactic plane. At these high frequencies, Faraday rotation effects can almost be neglected, which implies little depolarization by the interstellar medium along the line of sight. Thus the WMAP polarization data show intrinsic polarized emission. Their fractional polarization is rather low, and this should be the case at 1.4 GHz. In addition depolarization is important at 1.4 GHz, and it explains that the Galactic plane is almost invisible in polarization at 1.4 GHz. These results agree with the northern-sky survey by Wolleben et al. (2006), where the Galactic plane is also almost invisible due to depolarization.

## 2.3. Zero-level adjustment

While the Villa Elisa polarization survey was calibrated on an intensity scale using observations of extended polarized sources made with the Parkes telescope as described in Sect. 2.4, another important issue for the analysis of polarized diffuse Galactic emission is the determination of the correct zero-level (Reich 2006), which needs additional data. The southern sky lacks sensitive polarization data at an absolute level except for a few early measurements made with the Parkes telescope, and they are discussed in the following section. However, there is a significant overlap between declinations of  $-10^\circ$  and  $-29^\circ$  with the northern sky DRAO survey (Wolleben et al. 2006), which is tied to the absolute polarization level provided by the Dwingeloo data published by Brouw & Spoelstra (1976). We calculated the difference map in the region of overlap between both surveys in Stokes  $U$  and  $Q$ . The DRAO survey data for declinations between  $-27^\circ$  and  $-29^\circ$  are too incomplete and thus excluded for the present purpose. The difference data were averaged along

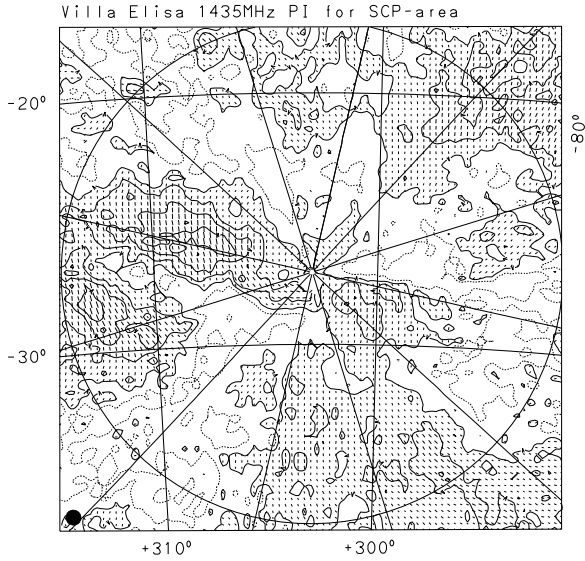


**Fig. 2.** 1.435 GHz polarized intensity for the SCP-area shown in Galactic coordinates. The contours start at 15 mK  $T_B$  and run in steps of 30 mK  $T_B$ . Polarization bars are in E-field direction and proportional to polarized intensities. They are shown above 45 mK  $T_B$ .

declination, and we adjusted the Villa Elisa maps at  $-10^\circ$  declination by the offset temperature profile in right ascension. However, this way small distortions of the DRAO survey introduce some stripe effects along declination since all the Villa Elisa scans were kept at the same South Celestial Pole (SCP) temperature at  $-90^\circ$ . Again the “unsharp masking” method was applied to remove these stripes.

The SCP polarization temperature at 1.4 GHz has not been measured so far, so that the accuracy of the offset level of the survey towards lower declinations is not known precisely. One constraint we have at present is based on the assumption that any astronomical structure in the SCP area should not show any peculiarity reflecting that all survey scans start at the SCP. We therefore transformed the equatorial  $U$  and  $Q$  data into Galactic  $U$  and  $Q$  data and checked the resulting polarized intensity image for possible weak gradients running towards the SCP. We finally corrected the original  $Q$  images for a gradient of 20 mK  $T_B$  and show the resulting polarized intensity image in Fig. 2, which proves that, except for a very small region of about  $2^\circ$  in diameter, the SCP region shows no unusual signature. A broad polarization structure runs across the SCP area with very little distortion whether in polarized intensity or in the distribution of the polarization angles. We are therefore confident that remaining offset levels and temperature gradients are small. In Sect. 3.1 we limit any temperature gradient to less than 30 mK  $T_B$  based on a comparison with WMAP polarization data.

#### 2.4. Comparison with Parkes 1.4 GHz southern sky polarization data

Compact and strong polarized sources suitable for polarization calibration with a small telescope are rare in the southern sky. We compared our polarization data with strong but extended polarized sources previously observed with the Parkes 64-m telescope, such as the radio galaxies Fornax A and Pictor (Gardner et al. 1975) and in particular with the strong, very extended, and highly polarized radio galaxy Centaurus A. From the comparison we found that the observed CH3 and CH4 polarization data

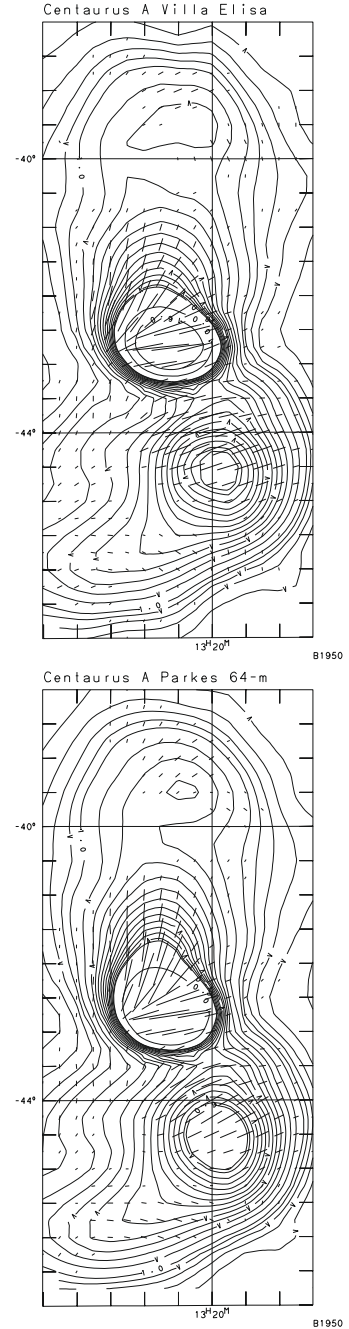


**Fig. 3.** Comparison of the 1.4 GHz Centaurus A map observed with the Parkes 64-m telescope smoothed to the Villa Elisa beam of  $36'$  and the map extracted from the Villa Elisa survey. Total intensity contours run in steps of 200 mK  $T_B$  (main beam temperature). Bars follow the B-field direction (assuming negligible Faraday rotation). Their length is proportional to polarized intensities and are shown for intensities exceeding 100 mK  $T_B$ .

relate to Stokes  $U$  and  $Q$  as CH3 =  $-U$  and CH4 =  $Q$  with a polarization angle correction by  $-23^\circ$ .

A new 1.4 GHz Parkes map (Junkes & Haynes, priv. comm.) including polarization was convolved to the lower angular resolution of  $36'$  of the Villa Elisa map and the resulting maps are both shown in Fig. 3. Both maps agree closely in total intensity and linear polarization. Small differences for the most intense parts indicate a different amount of residual instrumental polarization in the Parkes map and the cross-talk corrected Villa

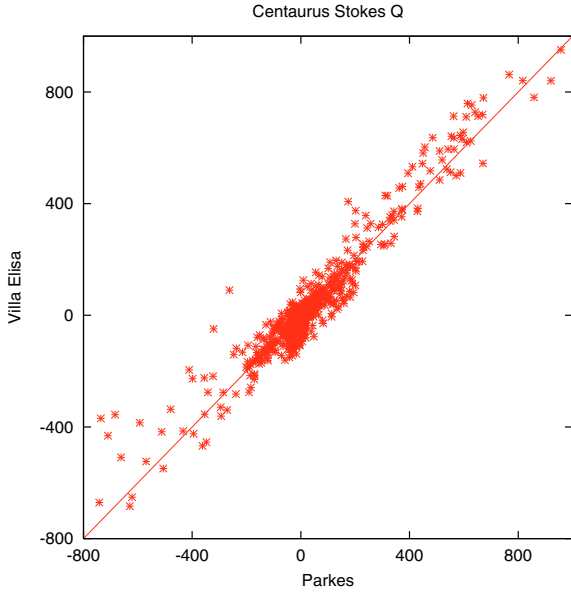


**Fig. 4.** Comparison of the Stokes  $Q$  intensities (in  $\text{mK } T_B$ ) of the Centaurus A maps shown in Fig. 3 at an angular resolution of  $45'$ . The line indicates the one-to-one correspondence of both measurements.

Elisa map. In general the polarization angle differences to all Parkes data used for calibration are within  $\pm 3^\circ$ , which we adopt as our polarization angle accuracy for polarized regions where the signal-to-noise ratio is high. We compare the measured  $Q$  data for Centaurus A from both telescopes in Fig. 4, and they agree quite well in general. Small pointing differences between the two maps and local small distortions in each map result in deviations of single pixels from a perfect one-to-one correspondence. A fit of the slope gives a coefficient of  $1.02 \pm 0.04$ .

Mathewson et al. (1966a) have carried out intensive polarization measurements of the southern sky at 408 MHz with the Parkes 64-m telescope and also made a few measurements at 1.4 GHz, which may be compared with data from the Villa Elisa survey. These early 1.4 GHz observations were limited in sensitivity, and the measured polarized intensities are given in units of  $50 \text{ mK } T_B$  after being multiplied by 0.5 according to the IAU adopted definition of linear polarization (see Berkhuijsen 1975, for details).

Mathewson et al. (1966b) list polarization measurements of diffuse emission at 37 positions distributed across the southern sky. We extracted the corresponding data for polarized intensity and polarization angle from the Villa Elisa survey. We excluded five measurements, which have exceptional large polarization angle differences between  $26^\circ$  and  $86^\circ$ . In addition, three of them have differences of more than  $100 \text{ mK}$  to the Villa Elisa data. Figure 5 shows a comparison between the polarized intensities of the remaining 32 values. Mathewson et al. (1966b) only published polarized intensities exceeding  $200 \text{ mK } T_B$  with an accuracy of  $50 \text{ mK } T_B$ . The mean value for the Villa Elisa data are 209, 238, and  $298 \text{ mK } T_B$  for the corresponding Parkes values of 200, 250, and  $300 \text{ mK } T_B$ . The agreement between the two sets of data is within a few percent. We also compared the polarization angles and find an average of the polarization angle differences of  $-0.5^\circ$ . Twenty of the 32 polarization angles agree within  $10^\circ$ . The centre frequency difference of both measurements is 25 MHz, which results in an angle difference of up to  $1^\circ$  for typical Galactic rotation measure values in the range of  $\pm 10 \text{ rad m}^{-2}$  (Spoelstra 1984). We conclude that, despite the

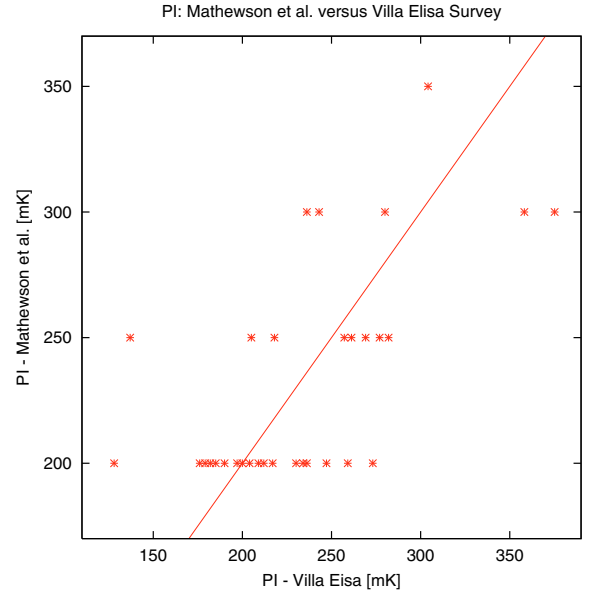


**Fig. 5.** Comparison of the polarized intensities as measured by (Mathewson et al. 1966b) with the Parkes telescope at 1.4 GHz with data extracted from the Villa Elisa survey. The Parkes data are published in units of  $50 \text{ mK } T_B$ . The line indicates the one-to-one correspondence of both measurements.

**Table 1.** Parameter of the Villa Elisa polarization survey.

Antenna diameter	30 m
Geographic location	$58^\circ 08' 25''.04, -34^\circ 51' 57''.35$
Coverage in RA	$0^{\text{h}}$ to $24^{\text{h}}$
Coverage in Dec	$-10^\circ$ to $-90^\circ$
$T_{\text{sys}}$	90 K
HPBW	$36'$
Sampling	$15'$
Centre frequency	1435 MHz
Bandwidth	14 MHz
Observing period	1987–1989
rms-noise $U, Q$	$\sim 15 \text{ mK } T_B$
Polarization angle error	$\pm 3^\circ$
Systematic zero-level error	$\leq 30 \text{ mK } T_B$
Pointing accuracy	$\pm 2'$

limited sensitivity of the early Parkes data, scaling and angle calibration of the Villa Elisa survey agree.

### 3. Results

Table 1 lists the basic parameters for the Villa Elisa polarization southern sky survey. Figures 6 and 7 shows greyscale coded Stokes  $U$  and  $Q$  maps in the equatorial coordinate system following in principle the presentation of the northern sky DRAO polarization survey by Wolleben et al. (2006) by considering the lower level of linear polarization in the southern sky. We measured a rms-noise in the  $U$  and  $Q$  maps of  $\sim 15 \text{ mK } T_B$ , which is at the same level as for the northern sky survey. In Fig. 8 the greyscale-coded polarized intensities  $PI$  are displayed, which were calculated from the  $U$  and  $Q$  intensities corrected for the positive noise bias following Wardle & Kronberg (1974):

$$PI = \sqrt{(U^2 + Q^2 - 1.2\sigma^2)} \quad (1)$$

where  $\sigma$  is the rms-noise measured from the  $U$  and  $Q$  maps. Figure 9 shows selected polarization E-vectors.

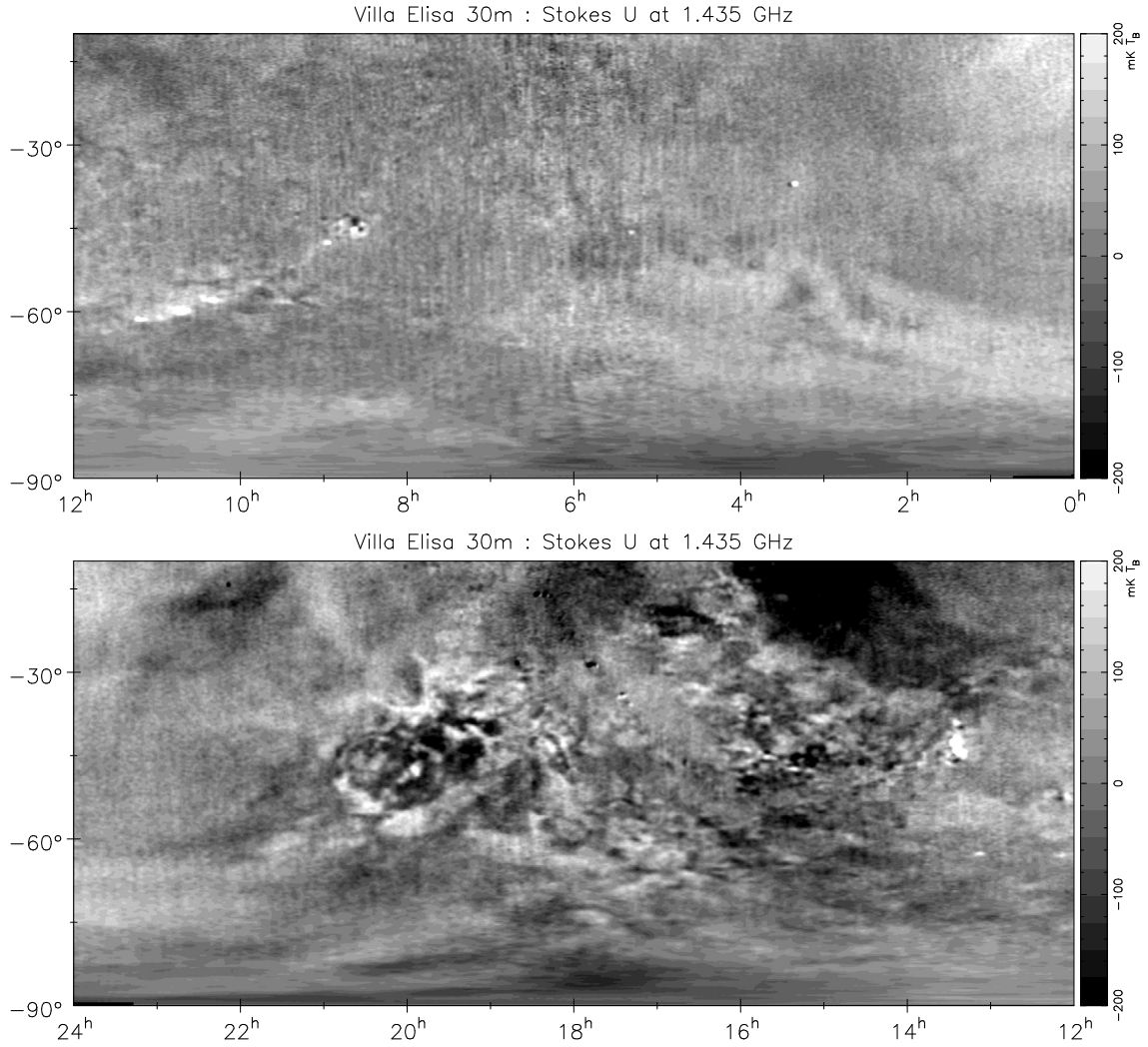


**Fig. 6.** Stokes  $U$  maps from the Villa Elisa 1.435 GHz polarization survey in equatorial coordinates (J2000).

The Villa Elisa survey data are accessible via the *MPIfR Survey Sampler*: <http://www.mpifr-bonn.mpg.de/survey.html>. Specified sections in various coordinate systems can be obtained in FITS- or NOD2-format. Also, GIF-images can be obtained.

### 3.1. Global polarization properties

The distribution of spectral indices for polarized intensities calculated from the 1.435 MHz Villa Elisa survey and the 22.8 GHz WMAP survey (Page et al. 2007) at an angular resolution of  $1^\circ$  is shown in Fig. 10. Most frequent spectral indices are between  $\beta = 2.8$  and  $\beta = 3.0$  with  $T_B(PI) \sim \nu^{-\beta}$ . Regions along the Galactic plane with  $|b| \leq 30^\circ$  are depolarized at 1.435 GHz and have flat spectra, while the spectral indices show a large scatter for regions with polarized emission close to the noise level, which results in very flat and very steep spectra. Outside of depolarized regions close to the plane the spectral distribution resembles the spectral index distribution for the corresponding total intensity emission (P. Reich et al. 2004). This is a strong indication that, at high Galactic latitudes, where Faraday rotation effects leading to depolarization are not significant at 1.435 GHz, the observed polarized intensities show the intrinsic Galactic polarized emission. The spectral index distribution shows no dependence on declination as expected. We checked the adopted SCP

temperature by adding a polarized intensity gradient from  $-10^\circ$ , where the survey is tied to the DRAO survey, to  $-90^\circ$ . A clear gradient of the average spectral indices in declination results when adding 30 mK  $T_B$  or more at 1.435 GHz. Thirty mK  $T_B$  is therefore the maximum zero-level uncertainty of the survey, as listed in Table 1.

We also calculated the percentage polarization of the 1.435 GHz southern sky survey at  $1^\circ$  angular resolution, together with the corresponding total intensity data (Reich et al. 2001), where 2.8 K have been subtracted to account for the isotropic CMB background emission and unresolved extragalactic sources. The histogram is shown in Fig. 11. It is evident that the percentage polarization is rather low in general, with a peak in the distribution around 5%. Only a small fraction of the pixels have percentage polarizations exceeding 20% and more, which is significantly below the intrinsic percentage polarization of synchrotron emission, and that is close to 75%. The polarized intensity spectrum shows that depolarization is not strong at 1.435 GHz for Galactic high-latitude emission. We conclude that this low percentage polarization is an intrinsic property of Galactic high-latitude emission. If depolarization by Faraday rotation is insignificant one possible explanation for a low percentage polarization might be small-scale magnetic field fluctuations within the beam size of the observations. Another explanation is the superposition of a number of synchrotron emission

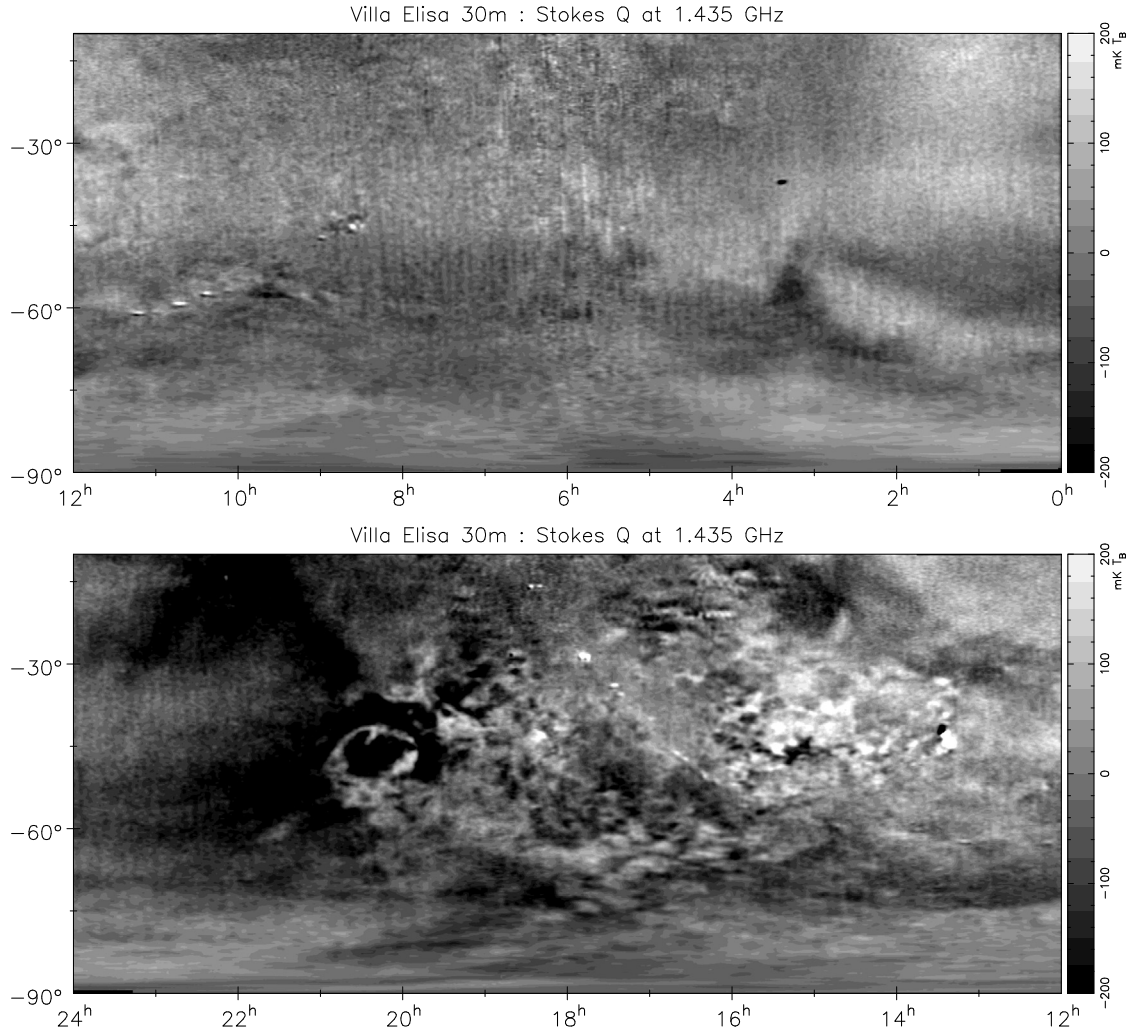


**Fig. 7.** Stokes  $Q$  maps from the Villa Elisa 1.435 GHz polarization survey in equatorial coordinates (J2000).

components along the line of sight, which have different orientations of the regular magnetic field direction.

### 3.2. The large high-latitude depolarized shell G353-34

Unbiased sky surveys are well-suited to revealing large extended structures out of the Galactic plane. A remarkable high-latitude depolarized structure is visible in the polarized intensity map and has already been mentioned by Testori et al. (2004). The polarized emission in this direction is enhanced for an area of about  $40^\circ \times 20^\circ$ . The shell-like structure is centered approximately at  $\alpha, \delta(2000) \sim 20^{\text{h}}25^{\text{m}}, -47^\circ$  or  $l, b \sim 353^\circ, -34^\circ$  and is denoted according to its Galactic coordinates G353-34. It has a diameter of about  $10^\circ$ . The object can be recognized well in the  $U$ ,  $Q$ , and  $PI$ , maps (Figs. 6–9). Very weak total intensity enhancement is associated with the depolarized shell, as shown in Fig. 12, which was extracted from the 1.4 GHz total intensity map (Reich et al. 2001) and smoothed to an angular resolution of  $2^\circ$ . Although the centre of the ring is at a high Galactic latitude, diffuse large-scale emission increasing towards the Galactic plane dominates, so it was removed by the application of the “background filtering technique” (Sofue & Reich 1979) using a filter beam size of  $5^\circ$ . We show 1.4 GHz total intensity contours after removal of the diffuse large-scale emission overlaid on polarized intensities in Fig. 12.

Two bisymmetric, total-intensity ridges follow the almost circular appearance in polarized intensity. This morphology suggests a possible identification as a supernova remnant (SNR), which according to its high latitude and large size, is very likely a local object with a diameter of  $D = 17.4 d_{100}$  pc at  $z = 57.4 d_{100}$  pc, where the distance  $d$  is in units of 100 pc. This object can also be clearly traced in the 408 MHz all-sky, total-intensity map of Haslam et al. (1982) when processed in the same way as the 1.4 GHz map. From a TT-plot analysis of the filtered total-intensity maps, we find a temperature spectral index  $T_B \sim \nu^{-\beta}$  of the shell that is  $\beta = 3.1 \pm 0.2$  between 408 MHz and 1420 MHz.

We also checked the WMAP 22.8 GHz total-intensity map (Hinshaw et al. 2007), but found no correspondence of the shell structure, which supports a steep non-thermal spectrum, as found for the lower frequencies, and clearly rules out a thermal origin of the shell. The non-thermal spectrum is steeper than for SNRs in the adiabatic expansion phase ( $\beta \sim 2.5$ ), and it indicates a SNR in the cooling phase, which means an evolved object. The depolarized shell is not visible in the WMAP 22.8 GHz linear polarization data (Page et al. 2007). No associated X-ray emission is evident from an inspection of ROSAT survey maps. A depression of diffuse infrared emission across the area of G353-34 is visible in the IRAS  $100 \mu\text{m}$  and  $60 \mu\text{m}$  maps. There is an indication for weak related HI emission in the southern sky

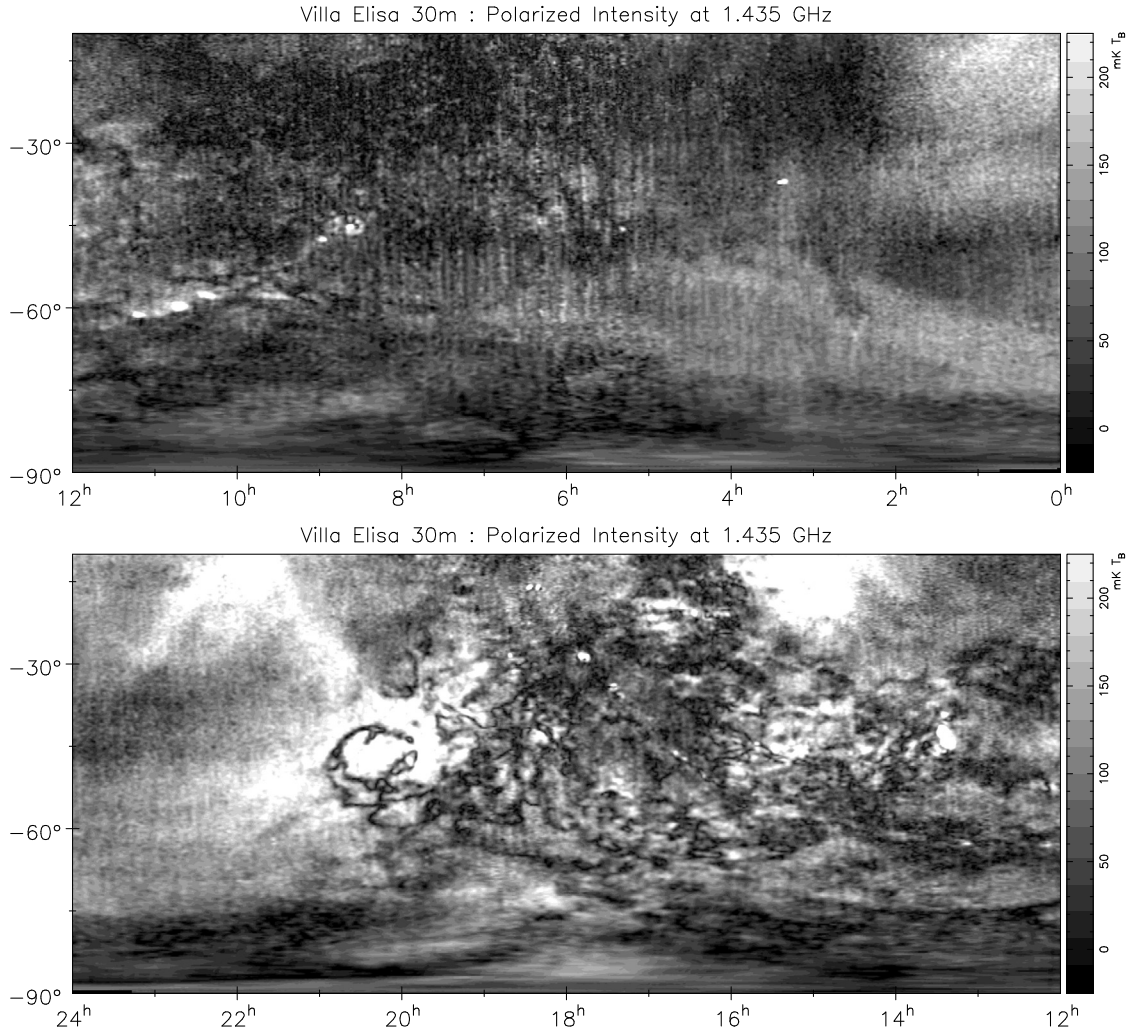


**Fig. 8.** Polarized intensity maps from the Villa Elisa 1.435 GHz polarization survey in equatorial coordinates (J2000).

HI survey by [Bajaja et al. \(2005\)](#). The HI velocity range is between  $4 \text{ km s}^{-1}$  and  $16 \text{ km s}^{-1}$ , which indicates that the shell is a local object. A detailed analysis of the HI data will be given elsewhere. Faint emission along the depolarized shell can be traced in the southern H $\alpha$ -survey (SHASSA) by [Gaustad et al. \(2001\)](#), when the large-scale diffuse background emission is filtered out and the map is smoothed to  $36'$ . We show the processed continuum-corrected H $\alpha$  emission overlaid on the polarized 1.4 GHz emission in Fig. 13. The depolarized shell is clearly traced by H $\alpha$  emission, which has a mean intensity of about 1 R, corresponding to an emission measure EM of  $\sim 2 \text{ cm}^{-6} \text{ pc}$ .

One explanation for the depolarization caused by the evolved SNR shell might be cancellation of diffuse Galactic polarization in its direction by the superposition with polarized shell emission at a different polarization angle. However, the total intensity emission of the shell is clearly weaker than the amount of polarized emission required, so this possibility can be ruled out. Associated H $\alpha$  emission may indicate enhanced Faraday rotation in the shell, which might act in two ways.

The amount of Faraday rotation might be such that polarized Galactic foreground emission cancels Galactic background emission. This kind of Faraday screen model was discussed previously by [Wolleben & Reich \(2004\)](#). In this particular case, the foreground and background components should be about equal, which means about  $100 \text{ mK } T_B$  to  $150 \text{ mK } T_B$ . This amount

of polarized foreground emission requires about  $200 \text{ mK } T_B$  associated total intensity synchrotron emission for a perfect organized magnetic field. For a more likely scenario with a less well-organized magnetic field, two or three times more synchrotron emission is required.

When we take the local excess of synchrotron emissivity into account ([Fleishman & Tokarev 1995](#); [Wolleben & Reich 2004](#)), we estimate the distance to the shell to be about 300 pc or 500 pc, which implies a shell diameter of about 50 pc to 85 pc. The tangential line of sight along the shell is estimated to be 30 pc to 55 pc for 5% shell thickness. For an EM of  $\sim 2 \text{ cm}^{-6} \text{ pc}$ , we calculate a thermal electron density between  $0.20 \text{ cm}^{-3}$  to  $0.26 \text{ cm}^{-3}$ . In this depolarization scenario a Faraday rotation of  $90^\circ$  or  $35 \text{ rad m}^{-2}$  has a maximum effect whenever foreground and background polarization angles take the same direction. We obtain a magnetic field component along the line of sight in the range of  $4 \mu\text{G}$  to  $6 \mu\text{G}$ , which is weak for an evolved SNR.

Finally we consider depolarization of background emission in the shell by high fluctuations of the magnetic field and/or the electron density in the shell on smaller scales than the angular resolution of the observations. This scenario, however, requires a very small distance for G353-34, because the foreground polarization along the shell is close to zero. Possibly a combination of the last two explanations describes G353-34 best; however,

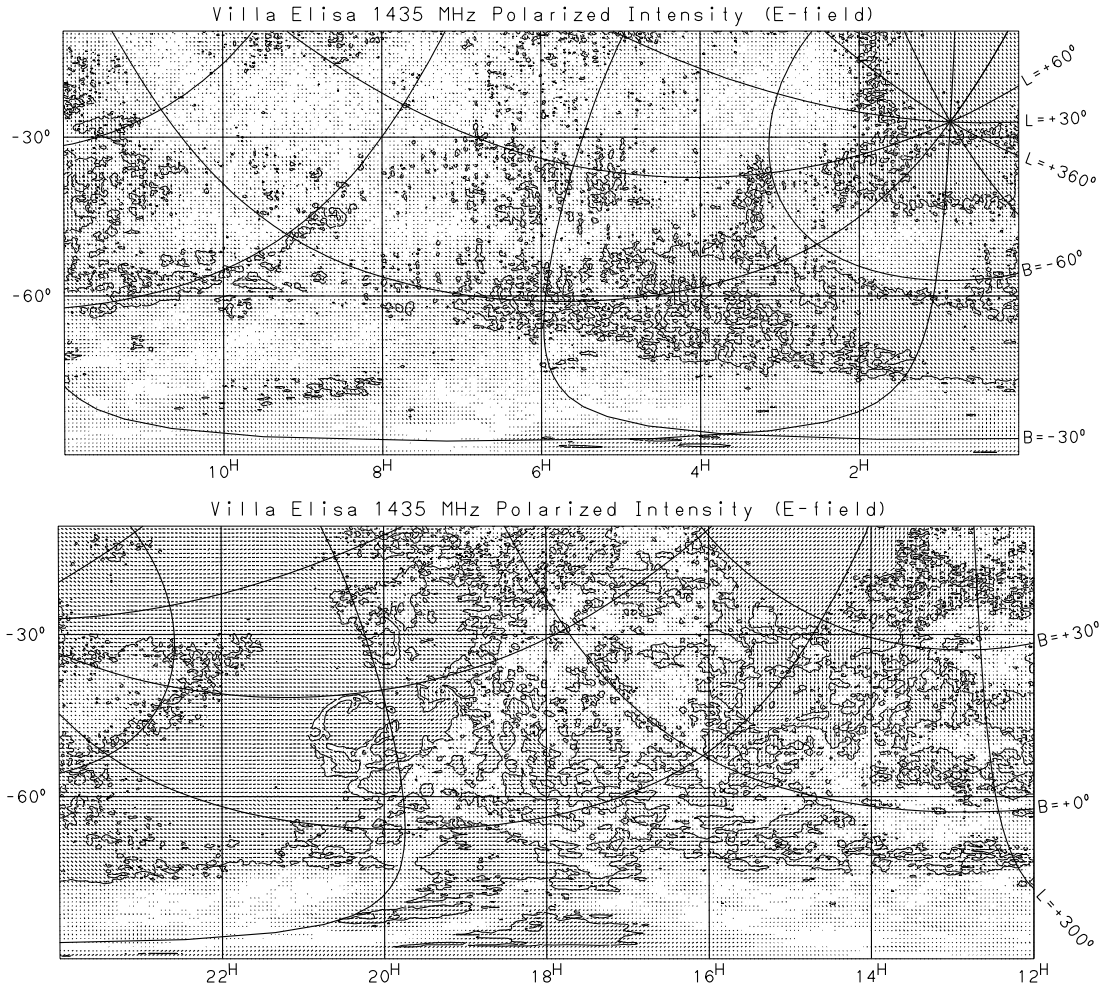


**Fig. 9.** Bars showing polarized intensities exceeding  $20 \text{ mK } T_B$  from the Villa Elisa 1.435 GHz polarization survey in equatorial coordinates (J2000). The overlaid polarized intensity contour is at  $100 \text{ mK } T_B$ . Also overlaid is the grid of Galactic coordinates.

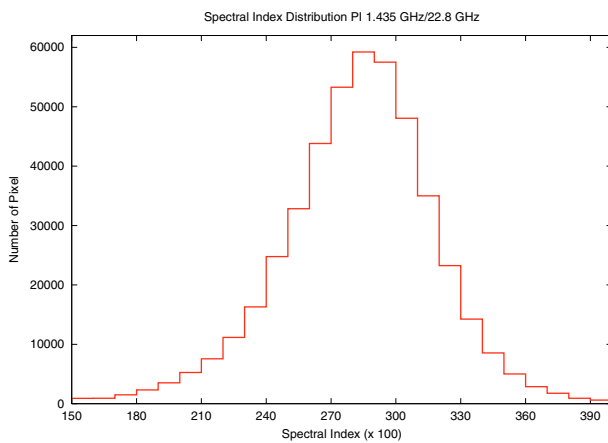


**Fig. 10.** Spectral index distribution for polarized emission between 1.435 GHz from the Villa Elisa survey and 22.8 GHz from WMAP.

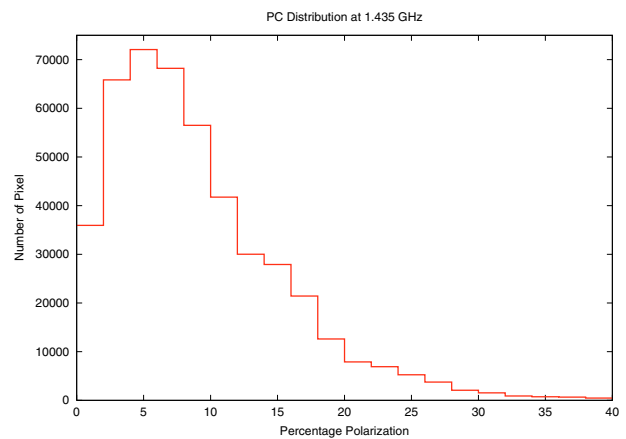


**Fig. 11.** The  $\lambda 21 \text{ cm}$  percentage polarization for the southern sky for declinations below  $-10^\circ$ .

without observations at more frequencies this cannot be investigated further.

#### 4. Concluding remarks

We have presented fully sampled maps of the linearly polarized intensities at  $\lambda 21 \text{ cm}$  for the entire southern sky below

declinations of  $-10^\circ$ . The absolute polarization level is obtained by adjusting the region of overlap between  $-10^\circ$  to  $-27^\circ$  with the northern-sky survey carried out at DRAO (Wolleben et al. 2006), which is tied to the absolutely calibrated polarization values of Brouw & Spoelstra (1976). The zero-level accuracy at lower declinations is better than  $30 \text{ mK } T_B$  or about twice the noise level. This polarization survey is the first one covering the

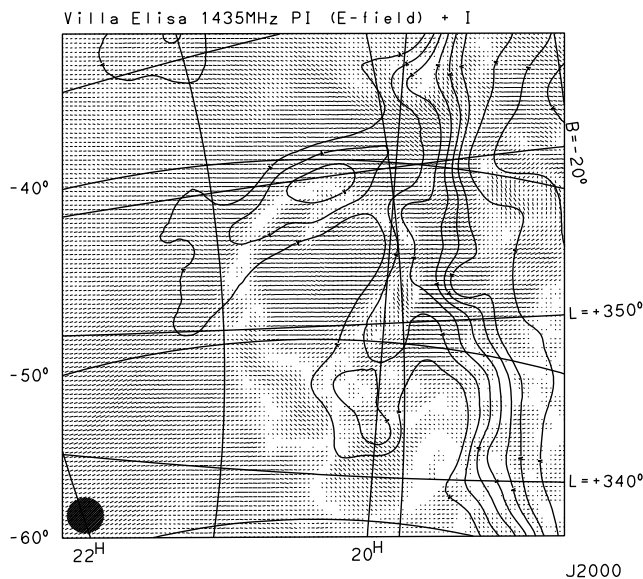


**Fig. 12.** Bars showing polarized intensities from the Villa Elisa 1.435 GHz polarization survey in equatorial coordinates (J2000) with overlaid contours of spatially filtered total intensities at  $2^\circ$  angular resolution (see Sect. 3.2). Contours start at  $25 \text{ mK } T_B$  and run in steps of  $25 \text{ mK } T_B$ . Polarized intensities exceeding  $50 \text{ mK } T_B$  are shown for every fourth  $15'$  pixel.

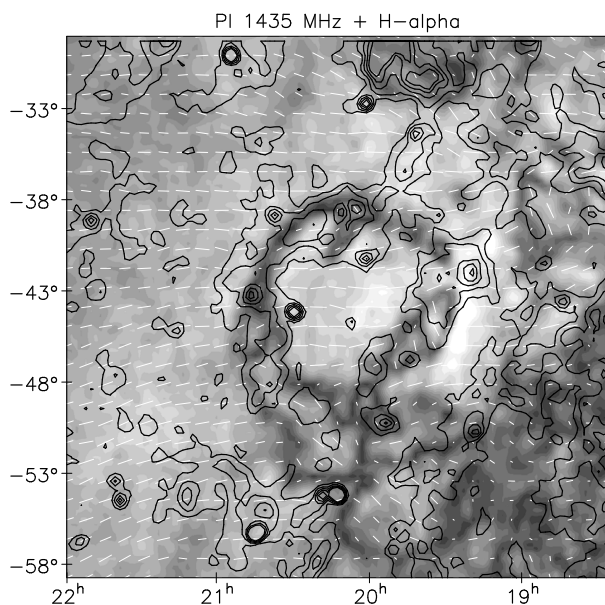


**Fig. 13.** Polarized 1.4 GHz emission (greyscale range from  $-100 \text{ mK}$  (black) to  $350 \text{ mK}$  (white)) and selected bars in E-field direction are shown, together with spatially filtered continuum corrected  $H\alpha$  emission from SHASSA overlaid. The contours are  $0.5 \text{ R}$  apart (see Sect. 3.2).

entire southern sky at that wavelength. Near the Galactic plane, the strong depolarization as seen for the northern sky is confirmed for the southern sky. Valuable information about the intrinsic Galactic polarization is provided by the recent high-frequency WMAP polarization all-sky maps (Page et al. 2007). Spectral indices for high-latitude polarized emission between 1.435 GHz and 22.8 GHz are close to those for total intensities, which indicates that low percentage polarization at 1.435 GHz is an intrinsic property of Galactic emission.

The polarized emission observed in the southern sky is much less contaminated by intensive large-scale structures as seen in the northern sky, e.g. by local structures like the North Polar Spur, Loop III, and the so-called “Fan region” centered at  $l \sim 140^\circ$  slightly above the Galactic plane. The southern sky is therefore better-suited for studies of the large-scale polarized cosmic microwave background than the northern sky. La Porta (2007) has made a comparative analysis of the angular power spectra of both the northern polarized sky (La Porta et al. 2006) and the southern polarized sky, and it reveals differences due to the local structures in the northern sky, which have an influence for latitudes of up to about  $60^\circ$ .

The combined all-sky map from the northern DRAO and the southern Villa Elisa 1.4 GHz polarization surveys will be presented in a forthcoming paper by Reich et al. (in prep.).

*Acknowledgements.* We would like to thank the staff at Villa Elisa for many years of technical support of these observations. J.C.T. is grateful to Richard Wielebinski for financial support to stay at the MPIfR Bonn. We thank Norbert Junkes and Ray Haynes for providing their Parkes 1.4 GHz map of Centaurus A prior to publication. We thank Marcelo Arnal for help with the HI data analysis of G353-34. We acknowledge the use of the Southern H $\alpha$  Sky Survey Atlas (SHASSA), which is supported from the National Science Foundation. We thank Tom Landecker for many helpful comments, which improved and clarified the text.

## References

- Bajaja, E., Arnal, E. M., Larrarte, J. J., et al. 2005, *A&A*, 440, 767  
 Berkuijzen, E. M. 1975, *A&A*, 240, 311  
 Brouw, W. N., & Spoelstra, T. A. Th. 1976, *A&AS*, 26, 129  
 Fleishman, G. D., & Tokarev, Yu. V. 1995, *A&A*, 293, 565  
 Gaensler, B. M., Dickey, J. M., McClure-Griffiths, N. M., et al. 2001, *ApJ*, 549, 959  
 Gardner, F. F., Whiteoak, J. B., & Morris, D. 1975, *Aust. J. Phys. Suppl.*, 35, 1  
 Gaustad, J. E., McCullough, P. R., Rosing, W., & van Buren, D. 2001, *PASP*, 113, 1326  
 Haslam, C. G. T., Wilson, W. E., Graham, D. A., & Hunt, C. G. 1974, *A&AS*, 13, 359  
 Haslam, C. G. T., Salter, C. J., Stoffel, H., & Wilson, W. E. 1982, *A&AS*, 47, 1  
 Hinshaw, G., Nolta, M. R., Bennett, C. L., et al. 2007, *ApJS*, 170, 288  
 Junkes, N., Fürst, E., & Reich, W. 1987, *A&A*, 69, 451  
 La Porta, L. 2007, Ph.D., Bonn University  
 La Porta, L., Burigana, C., Reich, W., & Reich, P. 2006, *A&A*, 455, L9  
 Mathewson, D. S., Broten, N. W., & Cole, D. J. 1966a, *Aust. J. Phys.*, 18, 665  
 Mathewson, D. S., Broten, N. W., & Cole, D. J. 1966b, *Aust. J. Phys.*, 19, 93  
 Page, L., Hinshaw, G., Komatsu, E., et al. 2007, *ApJS*, 170, 335  
 Reich, P., Testori, J. C., & Reich, W. 2001, *A&A*, 376, 861  
 Reich, P., Reich, W., & Testori, J. C., 2004, in *The Magnetized Interstellar Medium*, ed. B. Uyaniker, W. Reich, & R. Wielebinski, Copernicus GmbH, 63  
 Reich, W. 2006, in *Cosmic Polarization*, ed. R. Fabbri (Research Signpost), 91 [arXiv:astro-ph/0603465]  
 Reich, W., Fürst, E., Reich, P., et al. 2004, in *The Magnetized Interstellar Medium*, ed. B. Uyaniker, W. Reich, & R. Wielebinski, Copernicus GmbH, 45  
 Sofue, Y., & Reich, W. 1979, *A&A*, 38, 251  
 Spoelstra, T. A. Th. 1984, *A&A*, 135, 238  
 Sun, X. H., Han, J. L., Reich, W., et al. 2007a, *A&A*, 463, 993  
 Sun, X. H., Han, J. L., Reich, W., et al. 2007b, *A&A*, 469, 1003 (erratum)  
 Taylor, A. R., Gibson, S. J., Peracaula, M., et al. 2003, *AJ*, 125, 3145  
 Testori, J. C., Reich, P., Bava, J. A., et al. 2001, *A&A*, 368, 1123  
 Testori, J. C., Reich, P., & Reich, W. 2004, in *The Magnetized Interstellar Medium*, ed. B. Uyaniker, W. Reich, & R. Wielebinski, Copernicus GmbH, 57  
 Wardle, J. F. C., & Kronberg, P. P. 1974, *ApJ*, 194, 249  
 Westerhout, G., Seeger, C. L., Brouw, W. N., & Tinbergen, J. 1962, *Bull. Astron. Inst. Netherlands*, 16, 187  
 Wielebinski, R., Shakeshaft, J. R., & Pauliny-Toth, I. I. K. 1962, *The Observatory*, 82, 158  
 Wolleben, M., & Reich, W. 2004, *A&A*, 427, 537  
 Wolleben, M., Landecker, T. L., Reich, W., & Wielebinski, R. 2006, *A&A*, 448, 411